## Supplemental material

Mason et al., https://doi.org/10.1083/jcb.201806065

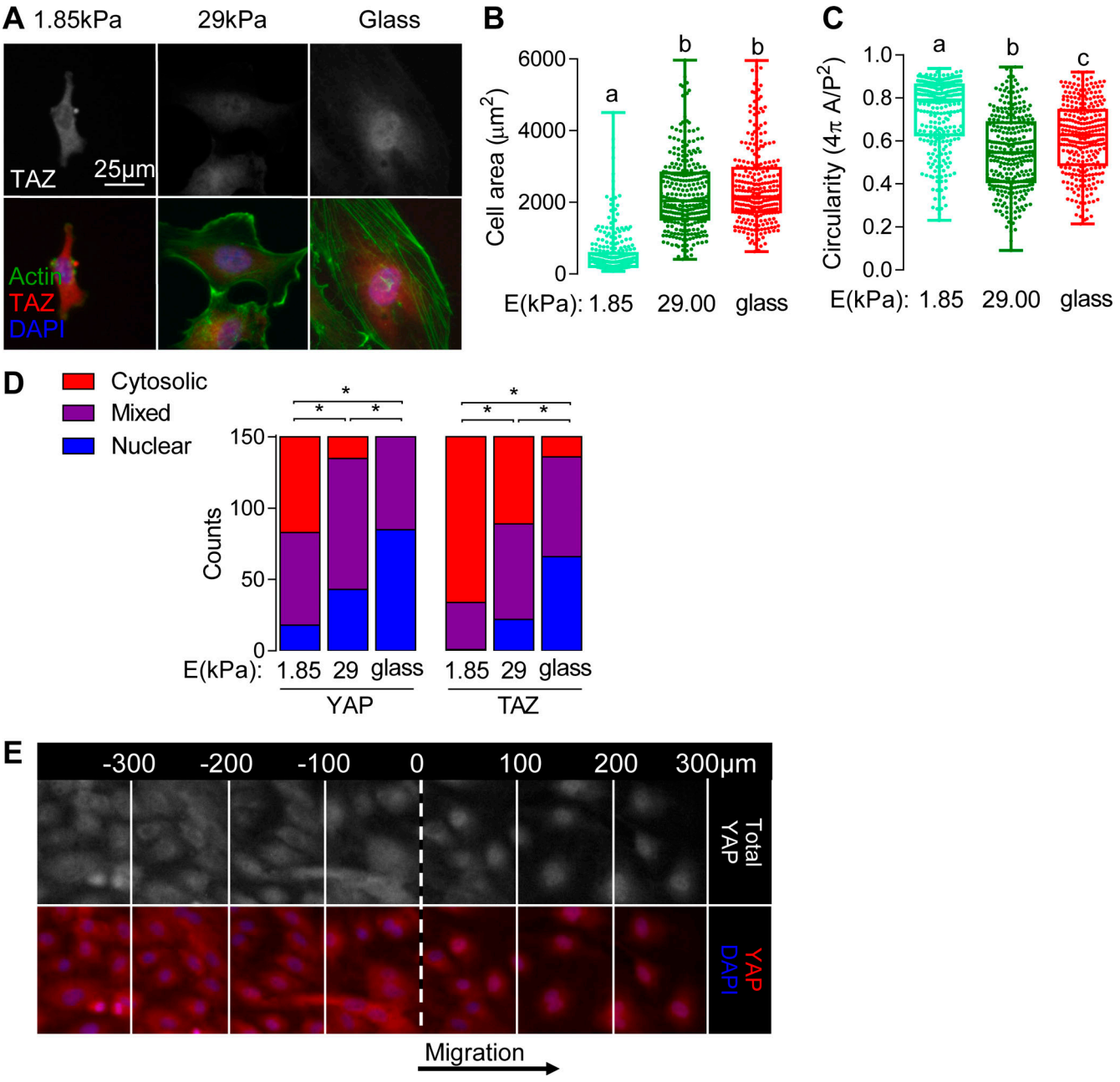


Figure S1. **YAP and TAZ nuclear localization are sensitive to rigidity in ECFCs.** ECFCs were seeded at 8.5 × $10^3$ cells per $cm^2$ on collagen-coated soft or stiff PA or glass for 24 h and then fixed and stained for YAP (not shown) and TAZ. **(A)** Representative images actin, TAZ, and nuclei visualized with Alexa Fluor 488– and 594–conjugated phalloidin and secondary and DAPI, respectively. **(B and C)** Individual cell area (B) and circularity (C) as a function of substrate elastic modulus. **(D)** Cumulative counts of YAP or TAZ subcellular localization based on qualitative assessment; $n$ = 150; $P < 0.0001$; $\chi^2$ test. **(E)** Representative immunofluorescent images of YAP localization visualized by Alexa Fluor 594–conjugated secondary and DAPI subdivided into 100-μm ROIs. Repeated significance indicator letters (e.g., a–a) signify $P > 0.05$, while groups with distinct indicators (a vs. b; *) signify $P < 0.05$. Summary statistics are represented as mean ± SEM. Box plots show interquartile range with whiskers at minimum/maximum.

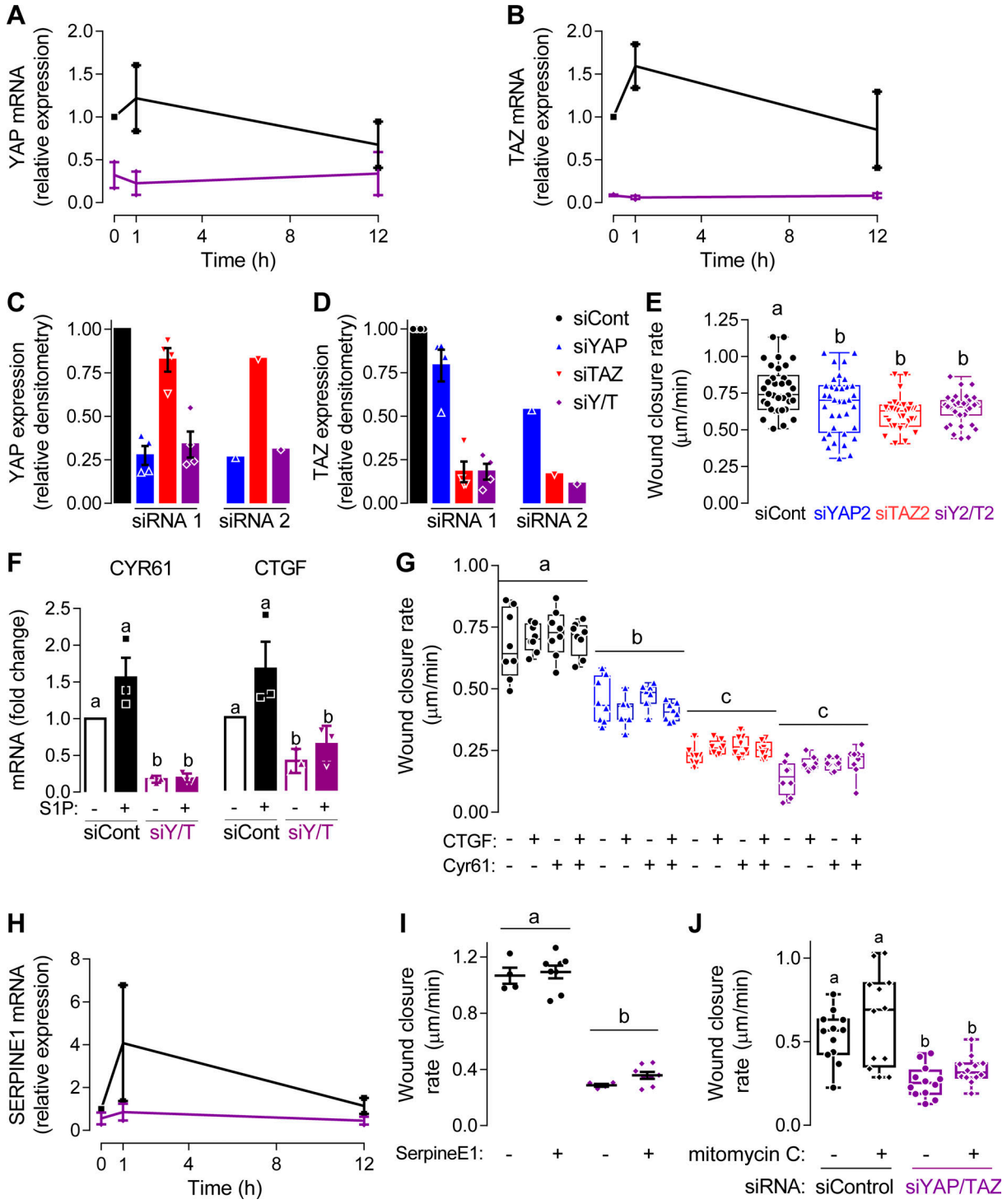


Figure S2. **Reconstitution of YAP/TAZ-dependent angiocrines CTGF, Cyr61, or SERPINE1 does not rescue ECFC migration.** Confluent ECFCs were scratched and lysate collected for gene expression 0, 1, and 12 h after initiation of migration. **(A and B)** *YAP* (A) and *TAZ* mRNA (B) expression in migrating ECFCs depleted of YAP and TAZ; $n = 4$. **(C and D)** YAP (C) and TAZ protein (D) expression after depletion with siRNAs 1 and 2. **(E)** Wound closure rate of confluent ECFCs imaged over 12 h after depletion of YAP and TAZ with siRNA 2; $n = 34$; $P < 0.01$; ANOVA with Tukey's post hoc test. **(F)** *CTGF* and *Cyr61* gene expression after treatment with sphingosine-1-phosphate for 1 h followed by lysis and RNA collection for RT-qPCR. $n = 2$ independent experiments; $P < 0.01$; ANOVA with Tukey's post hoc test. **(G)** Wound closure rate of cells treated with 50 and 100 ng/ml of CTGF and/or Cyr61. Groups treated with 50 or 100 ng/ml were combined for analysis, as there were no differences in wound closure between those treatments; $n = 7–8$; $P < 0.0001$; ANOVA with Tukey's post hoc test. Migrating ECFCs were lysed at 0, 1, and 12 h after the initiation of migration and lysate use for RT-qPCR. **(H)** *SERPINE1* gene expression during migration. $n = 2$ independent experiments. **(I)** Wound closure rate after treatment with 50 or 100 ng/ml of SERPINE1. Groups treated with 50 or 100 ng/ml were combined for analysis, as there were no differences in wound closure between those treatments; $n = 4–8$; $P < 0.0001$; ANOVA with Tukey's post hoc test. **(J)** ECFCs were pretreated with 20 μg/ml mito C during serum starvation, before initiation of cell migration. Wound closure rate (μm/min) was measured after 8 h; $n = 12$; $P < 0.02$; ANOVA with Tukey's post hoc test.

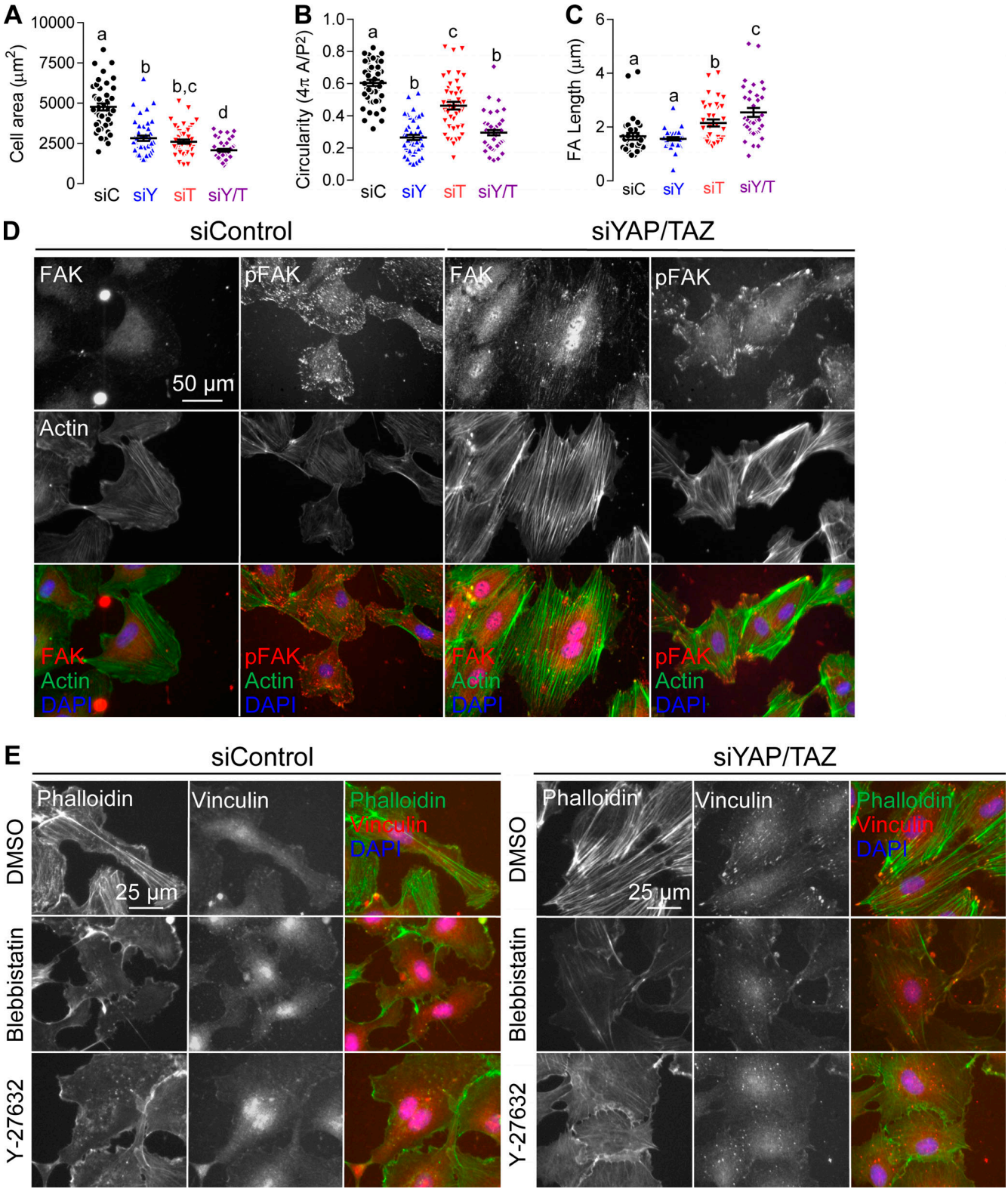


Figure S3. **YAP and TAZ depletion affects cytoskeletal and FA morphology by myosin activation and possibly by FAK localization.** Confluent ECFCs were scratched and allowed to migrate for 8 h then fixed for morphological analysis. **(A and B)** Cell area (A), $P < 0.004$, and circularity (B), $P < 0.0001$; $n = 45$; ANOVA with Tukey's post hoc test. **(C)** Average vinculin$^+$ FA length from data described in Fig. 6 C; $n = 33–35$; $P < 0.007$; ANOVA with Tukey's post hoc test. **(D)** Migrating ECFCs were fixed for immunofluorescence. FAK, pFAK, actin, and nuclei were visualized with Alexa Fluor 594–conjugated secondary, Alexa Fluor 488–conjugated phalloidin, and DAPI, respectively. **(E)** Vinculin and actin in migrating ECFCs visualized by Alexa Fluor 594–conjugated secondary and 488–conjugated phalloidin after treatment with ROCK inhibitor Y-27632 (10 μM) or Myosin II inhibitor Blebbistatin (20 μM).

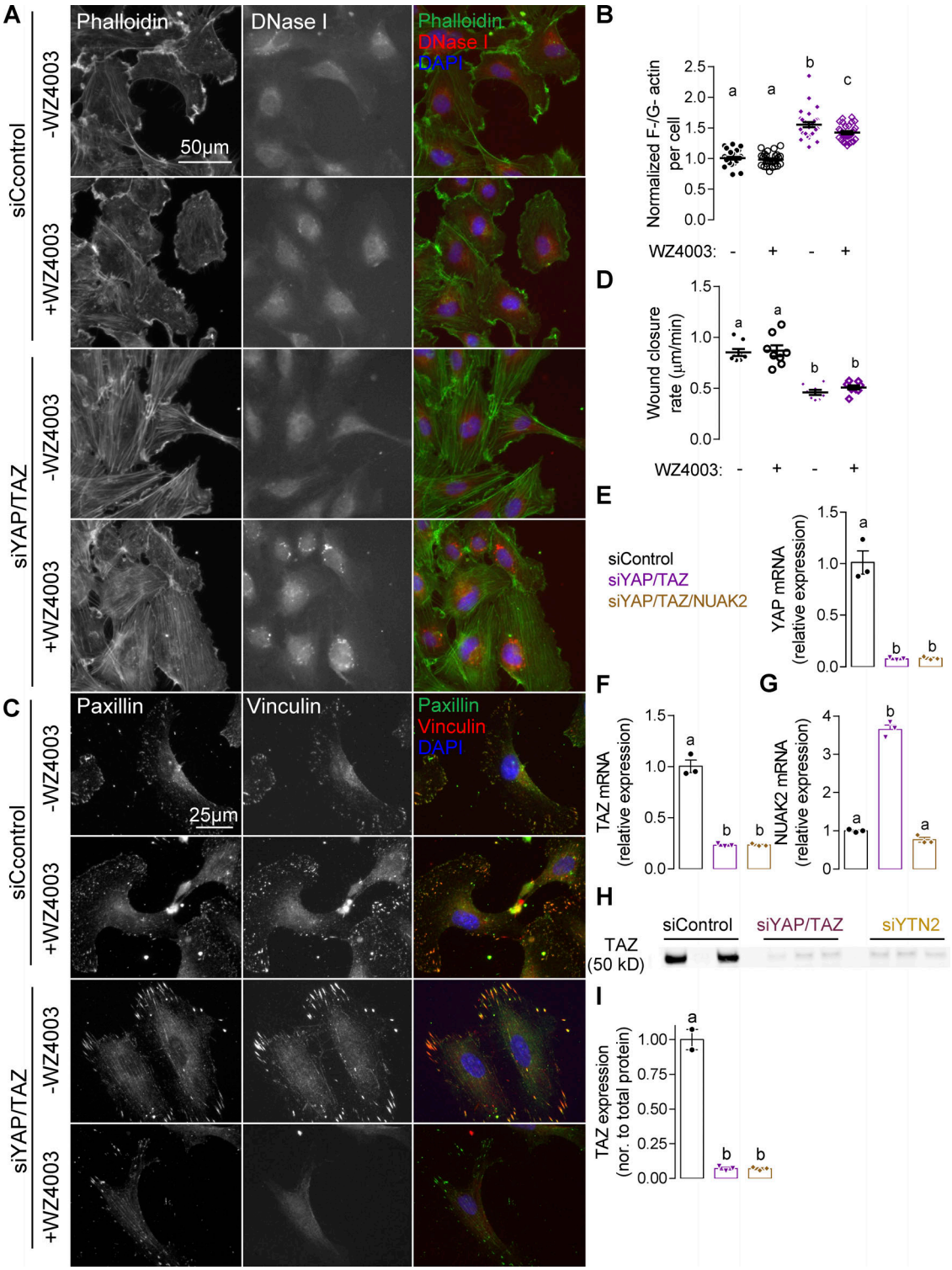


Figure S4. **NUAK2 inhibition with WZ4003 partially restores cytoskeletal defects in actin polymerization and F morphology but not migration in YAPR/TAZ-depleted cells.** Migrating ECFCs were depleted of YAP/TAZ and treated with 3 μM WZ4003, the NUAK2 inhibitor, for 8 h and then fixed for immunofluorescence. **(A)** Representative images of F- and G-actin visualized with Alexa Fluor 594–conjugated phalloidin and Alexa Fluor 488–conjugated DNase I. **(B)** F-actin fraction measured as phalloidin/DNase I intensity; $P < 0.04$; ANOVA with Tukey's post hoc test. **(C)** Representative images of vinculin and paxillin visualized with Alexa Fluor 594– and 488–conjugated secondary in QZ4003-treated cells. **(D)** Confluent ECFCs were scratched and imaged over 12 h and wound closure rate quantified. $n = 5–8$; $P < 0.0001$; ANOVA with Tukey's post hoc test. Efficiency of YAP and TAZ depletion is unaffected by codepletion with NUAK2, in addition to YAP and TAZ. **(E–G)** *YAP*, *TAZ*, and *NUAK2* mRNA expression relative to *GAPDH* measured by RT-qPCR after triple depletion of all three mRNA by siRNA; $P < 0.0001$; ANOVA with Tukey's post hoc test. **(H and I)** Western blot of TAZ expression after depletion of YAP, TAZ, and NUAK2 normalized to total protein; $P < 0.0001$; ANOVA with Tukey's post hoc test. Repeated significance indicator letters (e.g., a–a) signify $P > 0.05$, while groups with distinct indicators (a vs. b) signify $P < 0.05$.

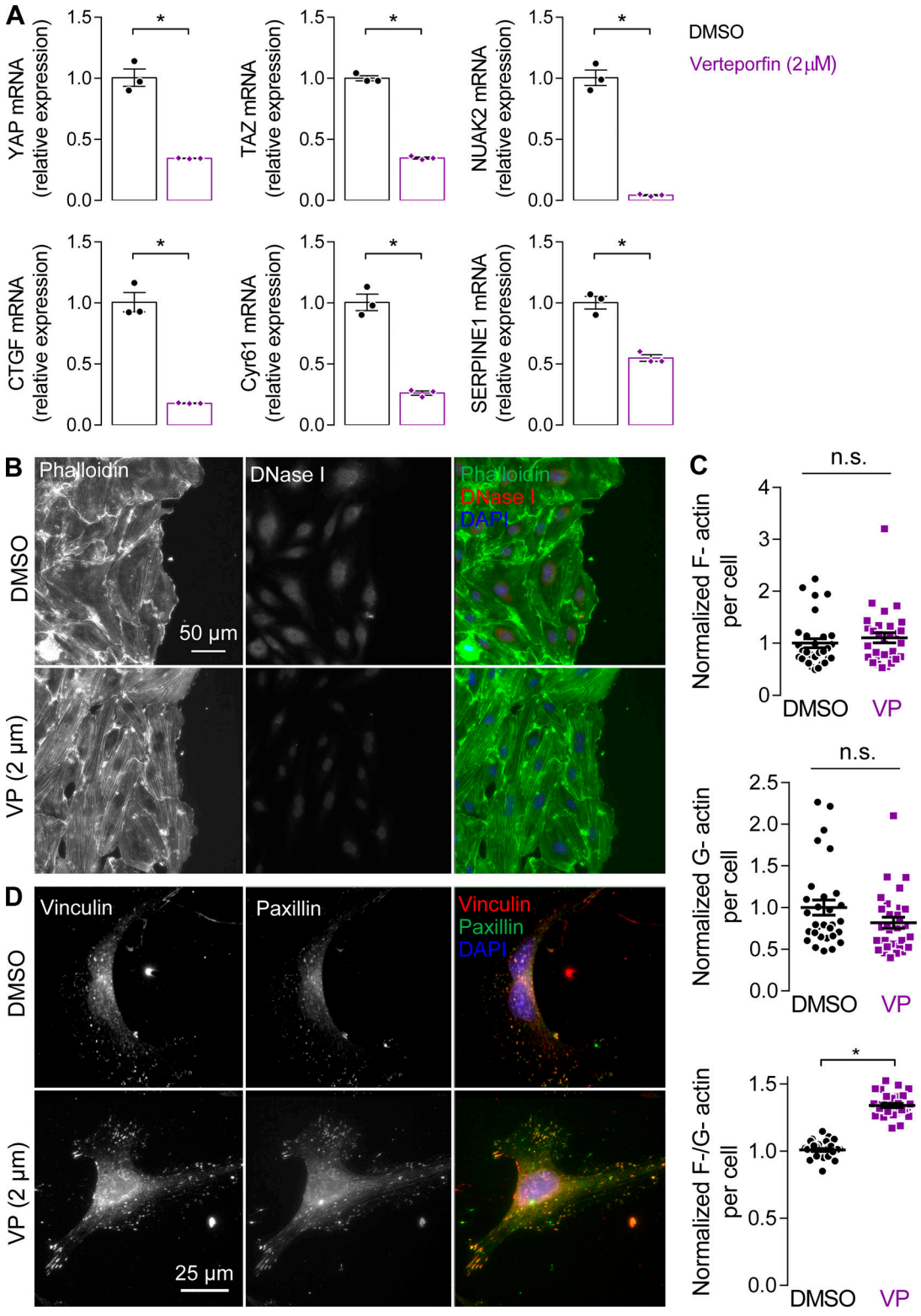


Figure S5. **Inhibition of the YAP/TAZ-TEAD interaction with VP phenocopies the cytoskeletal defects observed in YAP- and TAZ-depleted cells.** Migrating ECFCs were treated with 2 µM VP, the YAP/TAZ-TEAD interaction inhibitor, for 8 h then fixed for immunofluorescence or gene expression by RT-qPCR. **(A)** *YAP* and *TAZ* mRNA expression and YAP/TAZ target gene mRNA expression *NUAK2*, *CTGF*, *Cyr61*, and *SERPINE1*, measured relative to *GAPDH* by RT-qPCR; $P < 0.001$; two-tailed Student's unpaired *t* test. **(B)** Representative images of F- and G-actin visualized with Alexa Fluor 594–conjugated phalloidin and Alexa Fluor 488–conjugated DNase I. **(C)** Normalized F- and G-actin intensity ($P > 0.11$) and F-/G-actin ratio per cell, normalized to DMSO-treated controls. $n = 30$ cells; $P < 0.0001$; two-tailed Student's unpaired *t* test. n.s., not significant. **(D)** Cells were treated as described above and then Triton-extracted concurrent with fixation for immunofluorescence and analysis of structural FAs. Representative images of vinculin and paxillin visualized with Alexa Fluor 594– and 488–conjugated secondary, respectively. Significance indicator (*) signifies $P < 0.05$.

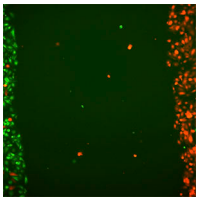

Video 1. **Live imaging of collective migration.** siControl (EGFP, left)- and siYAP/TAZ (mTomato, right)-treated ECFCs were seeded to confluence on collagen-coated plastic for 2 h in a custom polydimethylsiloxane stencil. Collective cell migration was tracked for 10 h in 15-min intervals.

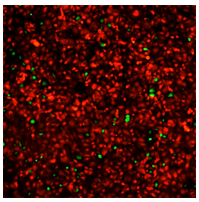

Video 2. **YAP/TAZ-depleted cell paracrine signaling has limited effect on control cell migration in a monolayer.** siControl (EGFP) were seeded 1:100 with siYAP/TAZ (mTomato)-treated ECFCs on collagen-coated plastic. Random migration in a confluent monolayer was tracked for 10 h in 15-min intervals.

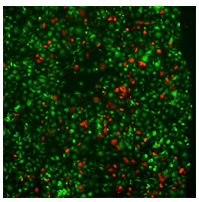

Video 3. **Control cell paracrine signaling does not rescue YAP/TAZ-depleted cell migration in a monolayer.** siYAP/TAZ (mTomato, right) were seeded 1:100 with siControl (EGFP)-treated ECFCs on collagen-coated plastic. Random migration in a confluent monolayer was tracked for 10 h in 15-min intervals.

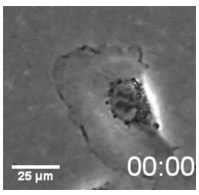


Video 4. **Control ECFCs have distinct lamellipodial protrusions.** Detailed phase contrast video of siControl-treated cell migration tracked for 10 min in 10-s intervals. Time is in min:s.

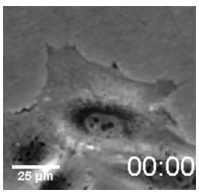


Video 5. **YAP/TAZ depletion causes significant membrane retraction.** Detailed phase contrast video of YAP/TAZ-depleted cell migration tracked for 10 min in 10-s intervals. Time is in min:s.